


Robust Methods for Automated Selection of Cardiac Signals After Blind Source Separation

Daniel Wedekind, Denis Kleyko, Evgeny Osipov , Hagen Malberg, Sebastian Zaunseder ,
and Urban Wiklund, *Member, IEEE*

Abstract—Objective: Novel minimum-contact vital signs monitoring techniques like textile or capacitive electrocardiogram (ECG) provide new opportunities for health monitoring. These techniques are sensitive to artifacts and require handling of unstable signal quality. Spatio-temporal blind source separation (BSS) is capable of processing suchlike multichannel signals. However, BSS's permutation indeterminacy requires the selection of the cardiac signal (i.e., the component resembling the electric cardiac activity) after its separation from artifacts. This study evaluates different concepts for solving permutation indeterminacy. **Methods:** Novel automated component selection routines based on heartbeat detections are compared with standard concepts, as using higher order moments or frequency-domain features, for solving permutation indeterminacy in spatio-temporal BSS. BSS was applied to a textile and a capacitive ECG dataset of healthy subjects performing a motion protocol, and to the MIT-BIH Arrhythmia Database. The performance of the subsequent component selection was evaluated by means of the heartbeat detection accuracy (ACC) using an automatically selected single component. **Results:** The proposed heartbeat-detection-based selection routines significantly outperformed the standard selectors based on Skewness, Kurtosis, and frequency-domain features, especially for datasets containing motion artifacts. For arrhythmia data, beat analysis by sparse coding outperformed simple periodicity tests of the detected heartbeats. **Conclusion:** Component selection routines based on heartbeat detections are capable of reliably selecting cardiac signals after spatio-temporal BSS in case of severe motion artifacts and arrhythmia. **Significance:** The availability of robust cardiac component selectors for solving permutation indeterminacy facilitates the usage of spatio-temporal BSS to extract cardiac signals in artifact-sensitive minimum-contact vital signs monitoring techniques.

Index Terms—Biomedical signal processing, blind source separation, cardiac signals, electrocardiogram, independent component analysis, permutation indeterminacy, sparse coding, spatio-temporal processing.

I. INTRODUCTION

THE telemedical management of early diagnosis and rehabilitation of diseases provides major opportunities for reorganizing an increasingly expensive healthcare system. Moreover, the ambulatory monitoring of health and stress offers new applications for monitoring people's wellness while performing safety-critical tasks, e.g. driving vehicles [1], [2].

Applicable ambulatory measurement techniques include dry-contact and noncontact biopotential electrodes [3]. Electrode implementations like textile or polymeric electrodes for wearable sensing or capacitive electrodes for seat-integrated sensing through clothes have been successfully proven to record the electrocardiogram (ECG) [1], [2], [4]. However, the recorded ECG is of non-standard nature when compared to its clinical counterpart. Moreover, the minimal-conductive measurement principle, which allows flexible health monitoring, is also strongly affected by movement artifacts [3]. The resulting decreased coverage and accuracy of a single channel can be addressed by exploiting the redundancy of a multichannel setup [4], [5].

Blind Source Separation (BSS) is a signal processing technique suitable for multichannel processing meanwhile aiming at the separation of signal mixtures (e.g., mixtures of ECG and distortions) into its components [6]. Whereas the standard BSS such as Independent Component Analysis (ICA) determines a purely spatial filter for processing multiple (spatially distributed) channels, the spatio-temporal BSS adds Finite Impulse Response (FIR) filters to the multichannel processing by adding a temporal dimension [7]. Spatio-temporal ICA-based on the FastICA algorithm [6] is one realization which has shown a superior performance on wearable data compared to the standard ICA [4].

In ICA settings for biomedical signal analysis, it is likely that the number of measured channels exceeds the number of underlying sources [8]. This is particularly relevant for ambulatory multichannel recordings. Most common ICA algorithms compute a symmetrical transformation, i.e., ensure the same number of input and output channels [8]. Since ICA is typically only solved up to a permutation (i.e., separated components are available but the output is unordered which is referred to as

Manuscript received June 19, 2017; revised September 23, 2017 and December 3, 2017; accepted December 20, 2017. Date of publication January 26, 2018; date of current version September 18, 2018. This work was supported by the Swedish Research Council under Grant 2015-04677. The work of D. Wedekind was supported in part by the Graduate Academy of the TU Dresden and in part by the Leonardo-Office Saxony (Erasmus+), which funded the short research stay in Umeå, Sweden, releasing this contribution. (Corresponding author: Daniel Wedekind.)

D. Wedekind is with the Institute of Biomedical Engineering, Technische Universität Dresden, Dresden 01062, Germany (e-mail: daniel.wedekind@tu-dresden.de).

H. Malberg and S. Zaunseder are with the Institute of Biomedical Engineering, Technische Universität Dresden.

D. Kleyko and E. Osipov are with the Department of Computer Science, Electrical and Space Engineering, Luleå University of Technology.

U. Wiklund is with the Department of Radiation Sciences, Biomedical Engineering, Umeå University.

Digital Object Identifier 10.1109/TBME.2017.2788701

permutation indeterminacy), the desired output component (e.g., the ECG component) has to be selected automatically. This selection is particularly important when processing a large number of channels as in spatio-temporal ICA, which adds time-lagged channels during the processing [7], [9], [10].

In the context of ECG processing and ECG identification, the permutation indeterminacy has been addressed by two major strategies. The first strategy aims at identifying the undesired components (i.e. artifacts) for exclusion, thus, it indirectly obtains the desired ECG component. Heuristic thresholds of second-order and higher-order statistics were used for that purpose in [11] whereas components periodicity by means of autocorrelation was exploited in [12]. Feature decision trees were used to classify artifacts in [13]. The second strategy aims at directly identifying the desired component (i.e. the ECG). Again, higher-order statistics have been utilized. Single channel selection by higher order moments was addressed in [4] and [14]. Multiple ECG candidates as input of a multichannel postprocessing were identified by utilizing kurtosis in [15]. Kurtosis ordering of heart activity components after ICA was used in [16]. Other approaches used template matching for single channel selection [17]–[19] and the amplitude of detected heartbeats [20]. A combination of both strategies, primarily sorting out undesired BSS components and further selecting the (best) ECG component among the residual channels, each utilizing frequency characteristics, was proposed by our group in [10] and [21].

Whereas the above described approaches directly measure signal statistics and features, component selection can also be based on more abstract signal representations. For instance, the ECG develops a characteristic and distinct waveform (the QRS complex) which marks the main excitation of the heart muscle and can serve as a basis of an abstract signal representation. After all, the periodic nature of this waveform under physiological conditions offers an indirect way of identifying the ECG component within a BSS output by assessing detections of QRS waveforms (peaks). The maternal ECG of an abdominal ECG recording after BSS was identified by comparing pre- and post-BSS QRS detections [22] or the assessment of QRSs' periodicity [23]. A simple periodicity criterion was also applied to identify the ECG component inside the BSS output of an electroencephalogram (EEG) by using QRS detections in [24]. A novel approach for evaluation of the temporal behavior of QRS detections by utilization of sparse coding was proposed by our group in [25].

If a temporal reference, e.g. the time instants of QRS complexes is available a priori, BSS can be applied with an additional constraint aiming at the temporal structure of the BSS output signal. The problem of component selection becomes obsolete. James and Gibson [26] identified the ECG component in the output after applying ICA to EEG by QRS time instants extracted from another simultaneously recorded signal. Lee *et al.* [27] realized the identification of the maternal ECG component from an abdominal ECG by using temporal a priori information. In this context, the signal covering the temporal constraint does not have to match the exact temporal behavior but should point the algorithm in the direction of the target component [8].

However, a priori information about temporal structures is more likely to be available in multi-diagnostic clinical settings rather than in contact-less recording settings.

Besides the existing diversified approaches to component selection, the evaluation of their actual selection performance is rare. Identifying a robust component selector would allow powerful techniques as spatio-temporal BSS to become applicable for multichannel biosignal processing. Accordingly, this study compares the performance of two novel automated BSS output selection approaches that are based on the temporal assessment of heartbeat (QRS) detections (proposed in its initial form in [24] and [25]) with the use of higher order statistics and time/frequency domain features in order to identify a single optimal ECG component. The novel approaches to solve permutation indeterminacy aim at directly identifying ECG components in BSS outputs based on a sparse representation of each component. The sparse representation itself, thereby, features QRS waveforms and their temporal behavior, expressed in the form of 'spike trains' typical for the spatio-temporal BSS on ECG [4]. The performance of the algorithms for BSS output channel selection is assessed using real ECG data of different origin (standard ECG, textile ECG, capacitive ECG), including recordings from both normal sinus rhythm and arrhythmia.

II. DATA MATERIAL

A. Textile ECG Data

The textile ECG (tECG) recordings consist of data from ten healthy subjects wearing a garment with integrated textile electrodes [4] while performing a protocol of motion and non-motion phases (sitting, standing, sitting down, standing up, walking, flexing chest muscles). Seven bipolar ECG leads obtained from the garment (sampling rate 500 Hz) using a reference potential near the waist were processed in subsequent 10s segments (1 s segment shift). A total of (mean \pm standard deviation) 536 ± 9 segments per subject were considered. Manual annotations in a reference ECG recorded simultaneously using conductive electrodes served as the ground truth. See Fig. 1(a) for a data example including a large motion artifact as well as Fig. 1(b) for an illustration of the electrode placement in the tECG garment.

B. Capacitive ECG Data

The capacitive ECG (cECG) recordings consist of data from ten healthy subjects seated at a driver's seat equipped with eight capacitive electrodes [10]. The protocol comprised a resting phase and a passive motion phase, where the seat was moved impulse-like from outside at a given period of time. Bipolar ECG leads were obtained using a fixed bipolar reference electrode in chest height. See Fig. 2(b) for an illustration of the electrode placement of the cECG system. Seven ECG leads obtained from the driver's seat (sampling rate 500 Hz) were processed in subsequent 10 s segments (1 s segment shift). A total of 523 ± 11 segments per subject containing both, resting and motion phases, were considered. The reference ECG recorded simultaneously using conductive electrodes served as

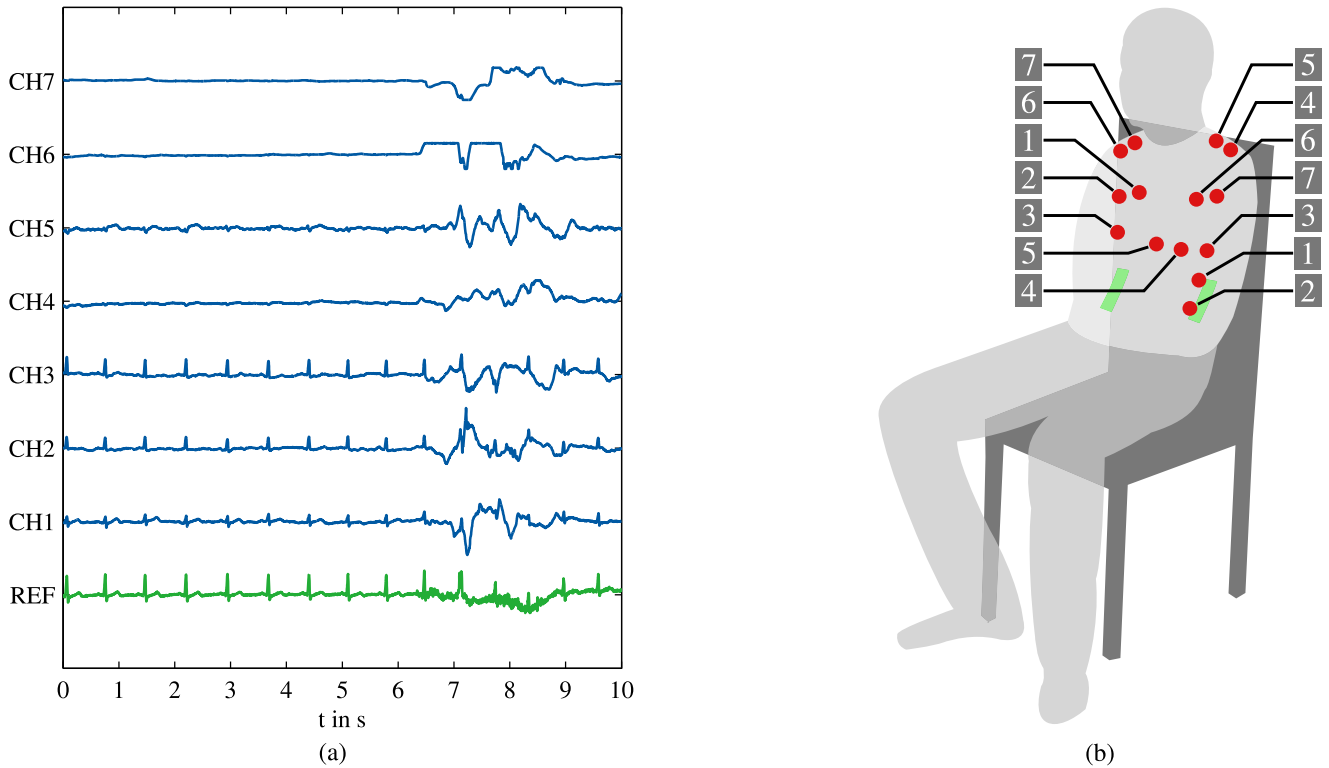


Fig. 1. Wearable data (tECG) and recording. (a) Input data with heavy distortions and a large motion artifact. REF indicates the conductive reference ECG and CH1-7 the ECG leads derived from the textile electrodes. Due to the normalization of signals, QRS complexes are not visible in the upper channels. (b) Electrode placement of the tECG garment. The numbered electrodes indicate pairs of bipolar leads (equivalent to CH in (a)) and the reference potential measurement is marked green near the waist.

the ground truth. See Fig. 2(a) for an example of a recording without a motion artifact.

C. Arrhythmia ECG Data

Since no arrhythmia data were available for the used tECG and cECG techniques, pathological (arrhythmia) ECG data (aECG) were assembled out of the PhysioNet [28] MIT-BIH Arrhythmia Database [29]. To match the data amount and the structure of the textile and capacitive ECGs, 100 segments (10 s duration, minimum 1 s segment shift, sampling rate 360 Hz) were randomly sampled out of each of the database's 48 ambulatory two-channel recordings. Based on the expert beat annotations available with the database, first, segments containing pathological beats (i.e. premature and block beats, no escape beats) were extracted. If 100 different segments containing pathological beats could not be sampled for a single patient, segments containing only (quasi-)physiological beats (sinus or paced beats) are added. By applying this procedure, we obtained 74 ± 41 of 100 segments for each patient containing pathological beats. The expert beat annotations also served as the ground truth regardless of its beat type.

III. DATA PROCESSING AND PERFORMANCE EVALUATION

A. Blind Source Separation

Each channel of each segment of the ECG data was normalized for further processing by subtracting its mean and

division through its standard deviation. Time-delayed versions of the original signals were added as additional inputs to the multichannel filter. The filter coefficients were determined by spatio-temporal ICA, which has shown superior performance compared to the standard ICA in the textile ECG setting [4]. Therefore, this BSS algorithm was exclusively selected for further processing. Spatio-temporal BSS using FastICA algorithm with the Skewness maximization and ten added time lags [10] ($k \in [0, 10]$ samples) was symmetrically applied to the seven textile or capacitive ECG leads which resulted in 77 output components per segment. Two ambulatory ECG leads of the arrhythmia database were processed similarly producing 22 output components per segment. In this context, the concept of Skewness maximization by BSS refers to generating spike train signals out of the ECG which show distinct QRS spikes and a low noise level. Fig. 3 shows an example of an output component excerpt of the tECG data according to the input data in Fig. 1(a).

B. Output Component Selection Using Heartbeat Detections

A component selection which is based on heartbeat detection consists of three major steps: 1) detection of peaks (both heartbeats and other peaks as large artifacts) in the output components; 2) interpreting the temporal behavior of the peaks of each component; 3) selecting one single component based on the

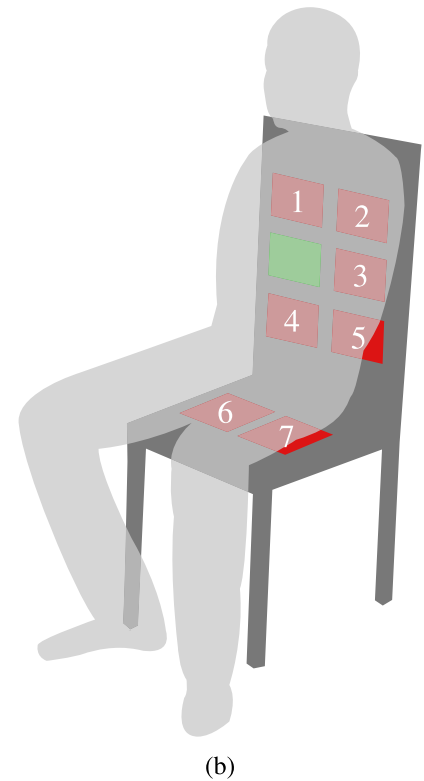
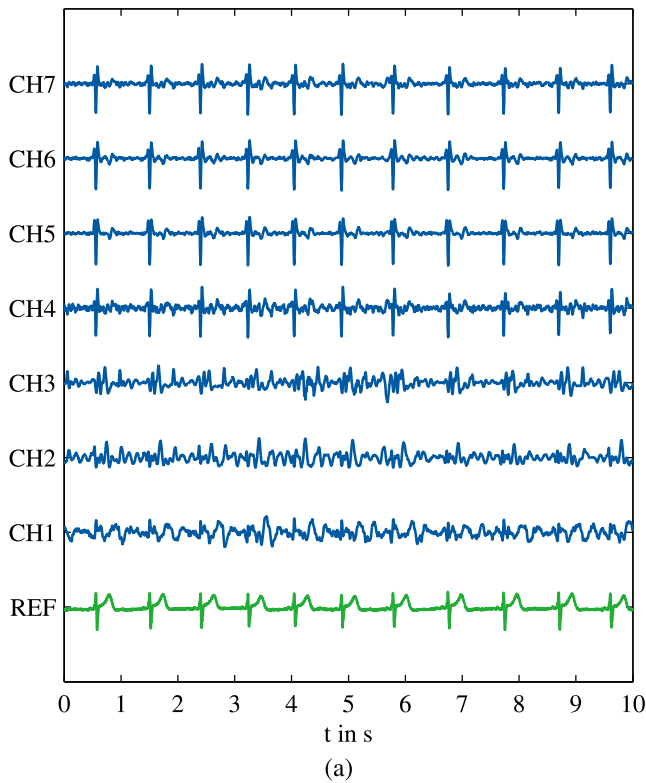


Fig. 2. Capacitive data (cECG) and recording. (a) Input data example of the capacitive data. REF indicates the conductive reference ECG and CH1-7 the ECG leads obtained from the driver's seat electrodes. (b) Electrode placement of the cECG setup. The numbered electrodes each define a bipolar lead (CH) together with the green (unnumbered) electrode.

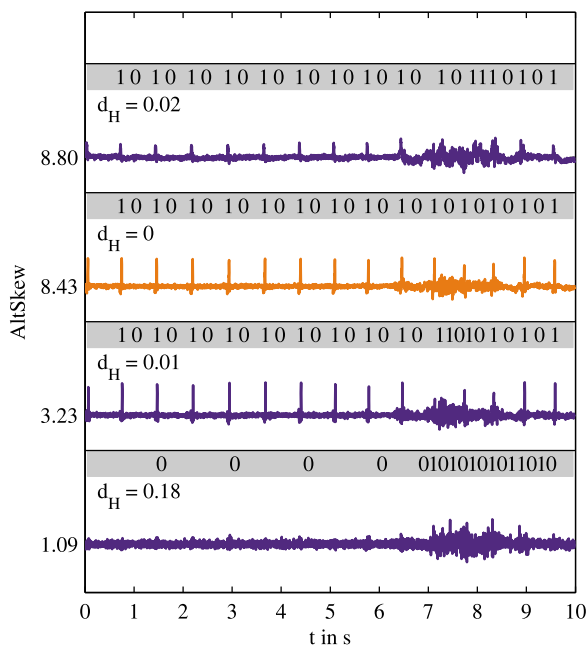


Fig. 3. Spatio-temporal BSS output components (excerpt) of the input signals from Fig. 1(a). Components are vertically ordered according to the alternative Skewness measure (AltSkew). The modified Hamming distance d_H as well as the sparse code sequence of each output component are shown in grey bars. The RCODE selection is marked by orange color and $d_H = 0$.

above interpretation which most likely resembles the noise-free ECG component. Note that the second step requires an analysis of heartbeat dynamics that includes both false positive and false negative detections.

Before the peak detection, each component was pre-processed by highpass-filtering (0.5 Hz, 5th-order Butterworth) and lowpass-filtering (40 Hz, 5th-order Butterworth), a subsequent normalization (subtraction of the mean and division by its standard deviation) and an optional sign-change to ensure consistent positive heartbeat peaks.

1) Peak Detection in BSS output components: The main function of the peak detection in this context is to serve the basis for a sensitive subsequent interpretation, thus achieving a balance between sensitivity to distortions and likewise the ability to detect peaks in the presence of distortions. The essential processing steps prior to peak detection are shown in Fig. 4. First, the envelope (ENV) is calculated for each BSS component using Hilbert transformation. A spike train signal is formed by extracting (EXT) the signal content above the lowpass-filtered (0.5 Hz, 5th-order Butterworth) envelope. This procedure intends to suppress distortions typical for relative motions between electrode and body surface in minimal-conductive ECG recordings (see Fig. 1(a) for an example). Peaks are further consolidated by moving window integration (MOV) using a 0.1 s Hamming window (considered as QRS length [30]). Finally, peaks are detected by applying our customized QRS-detector

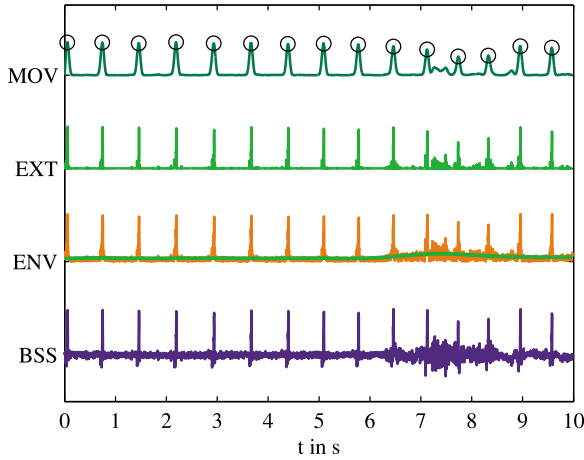


Fig. 4. Data processing steps prior to the coding. Spatio-temporal BSS output channel (BSS) including its envelope (orange) and the lowpass-filtered (green) envelope (ENV), the extracted signal (EXT) and its moving window integrated version (MOV) including peak detections (black \circ).

of the combined maximum-search [31] and the Pan-Tompkins [32] principle on MOV.

Specifically, the 'spike trains' typical for spatio-temporal BSS processing are robustly addressed by the detection principle of the simple maximum search detector [31]. However, the broad range of heart rates covered by the data as well as the arrhythmic events render the fixed heart rate guess of the maximum search detector to be impractical. Therefore, we combined the maximum search detector with the beat-to-beat decision logic and threshold-adaption of the Pan-Tompkins QRS-detection algorithm detecting one beat after another [32].

Whereas for the later assessment of the component selection a refractory period of 0.3 s was utilized on the original BSS component, the QRS-detector's refractory period was decreased to 0.05 s prior to the selection on MOV to achieve sensitivity to artifacts.

2) Interpretation of Peak Detections I (RCODE): In order to interpret the peak detections from the above procedure, we applied two different algorithms. The first (RCODE) was initially proposed by our group in [25]. It delivers a quasi-continuous measure between the expected behavior of a cardiac component consisting of peak detections followed by a reasonable time between subsequent peaks and differently pronounced deviations from this behavior up to a lack of multiple detections. This measure refers to as modified Hamming distance. It is derived from a sparse code representation of the peak detections. The distance is calculated for each component's peak detections at times t_i ($i \in [1, I]$, I is the number of peak detections) by coding according to the dictionary {peak - 1, no peak - 0} together with physiological temporal a-priori information. The cardiac refractory period Δt_R is considered as 0.3 s [22], whereas the maximum peak-to-peak distance Δt_{\max} is considered as 1.5 s (i.e. a minimum heart rate of 45 bpm [33]). Accordingly, a sequence $(x) \in \{0, 1\}$ is obtained by:

- 1) $(x_i) = 1$ with $i \in [1, I]$
- 2) add $\lceil (t_{i+1} - t_i) / \Delta t_{\max} \rceil$ zeros between x_i and x_{i+1} if $t_{i+1} - t_i > \Delta t_R$
- 3) add $\lfloor t_1 / \Delta t_{\max} \rfloor$ zeros to (x) at $t < t_1$
- 4) add $\lfloor (10 - t_I) / \Delta t_{\max} \rfloor$ zeros to (x) at $t > t_I$.

The sequence (x) of final length L is further evaluated by the modified Hamming distance d_H which is designed to indicate the distance from the expected code behavior assuming a perfect ECG component with code $(x) = 1, 0, 1, 0, \dots$ or $(x) = 0, 1, 0, 1, \dots$, respectively.

However, subjects with very low heart rate (≈ 45 bpm) or arrhythmia even under perfect peak detection ($\text{ACC} = 1$) can feature sparse code patterns like $(x) = \dots, 1, 0, 0, 1, \dots$ or $(x) = 0, 0, 1, \dots$ and $(x) = \dots, 1, 0, 0$ at the beginning/end of the code sequence, respectively. To avoid negatively judging codes of such origin, these patterns are identified in each output component of a segment. Moreover, if there is temporal coincidence of these patterns (< 50 ms) in multiple components of the same segment, very low heart rate or arrhythmia is considered to be apparent in the segment. One "0" of the respective (0, 0) code pairs is removed from the sequence (x) of the affected components in the case that none of the other components has already shown perfect ($(x) = 1, 0, 1, 0, \dots$) behavior.

After completing the code generation and manipulation, the modified Hamming distance distinctly evaluates single code pairs whether they show desired or non-desired patterns with respect to the expected cardiac pattern. Contrary to that, a common Hamming distance would serve a simultaneous distance measure between all code elements and the expected binary pattern. Our modified assessing measure d_H consists of two factors

$$d_H = w_d \cdot d_{10} \quad (1)$$

where d_{10} forms a distance to the expected behavior assessing only pairs of two subsequent code elements (x_i, x_{i+1}) each. It is defined by the ratio between the amount of non-desired code pairs (0, 0) or (1, 1) and the total amount of code pairs

$$d_{10} = \frac{|\{(x_i, x_{i+1}) | (x_i, x_{i+1}) = (0, 0) \cup (1, 1)\}|}{L - 1} \quad (2)$$

with $i \in [1, L - 1]$.

w_d factors the length of the longest continuous sequence $(x_i, x_{i+1}, \dots) \subseteq (x)$ of the expected ECG code behavior where all pairs of subsequent code elements suffice $(x_i, x_{i+1}) = (1, 0) \cup (0, 1)$. Accordingly,

$$w_d = 1 - \frac{l_{10}}{L - 1} \quad (3)$$

where l_{10} is the length of the longest continuous sequence. If $I = 1$, d_H is set to 1. Examples of code sequences (x) and derived distance measures d_H are shown in Fig. 3.

3) Interpretation of Peak Detections II (PeriodTest): The second algorithm is a simple periodicity test (PeriodTest) based on the peak detection evaluation proposed by Hamaneh *et al.* [24], which aims at the binary classification into periodic and non-periodic detections. It consists of the following three

conditions for classifying a series of peak detections at times t_i ($i \in [1, I]$, I the number of peak detections) and the series of the according inter-beat intervals (Δt in s) with $\Delta t_i = t_{i+1} - t_i$ and its median Δt_{med} as periodic (and non-periodic otherwise):

- 1) $1/\Delta t_{med} \geq 2/3$
- 2) $1/\Delta t_{med} \leq 3$
- 3) $|\{\Delta t_i | \Delta t_i < 0.75 \cdot \Delta t_{med} \cup \Delta t_i > 1.25 \cdot \Delta t_{med}\}| < 0.2 \cdot (I - 1)$

Besides the frequency limitation with respect to the median peak-to-peak interval, the amount of single peak-to-peak intervals deviating more than 25% from their median is limited to 20%. The result of the periodicity test is given as Hamaneh criterion $HC = 0$: periodic peak detections (cardiac component candidate) or otherwise $HC = 1$: non-periodic peak detections (other component).

4) Selection: The component with the minimal d_H or Hamaneh criterion $HC = 0$ is selected as RCODE or PeriodTest output, respectively. In the case of obtaining multiple components with equal minimum d_H or HC, a further selection is necessary to obtain a single output component for each selection routine. By application of spatio-temporal BSS with Skewness maximization, we are aiming at ‘spike trains’ as cardiac output components. In order to evaluate the quality of the spike train in cardiac component candidates, we apply a measure similar to Skewness but focused on the peaks only. A peak energy vector E_p is formed by the maximum peak value of the preprocessed component around each peak detection $E_{p,i} = \max_{t_i \pm 25 \text{ ms}}(BSS)$. The *AltSkew* measure assesses the average absolute peak energy of $E_{p,i}$ divided by its standard deviation:

$$AltSkew = \frac{\frac{1}{I} \sum_{i=1}^I |E_{p,i}|}{\sqrt{\frac{1}{I-1} \sum_{i=1}^I (E_{p,i} - \bar{E}_p)^2}}. \quad (4)$$

Accordingly, highly energetic peaks of similar amplitude provide a high *AltSkew*. Examples can be seen in Fig. 3, where components are vertically ordered with respect to *AltSkew*. Among the components with equal minimum d_H or HC, the single component with the maximum *AltSkew* is selected.

C. Output Component Selection by Standard Approaches

In order to facilitate a comparison to traditional component selection methods using higher-order statistics [4], [11], [14]–[16], we also applied a single component selection based on Skewness and Kurtosis, respectively. To achieve measures which are less affected by outliers, an outlier-removal using Walsh’s non-parametric outlier test [34] was performed on each component prior to selecting the component with the highest Skewness (SKEW) or highest Kurtosis (KURT).

Additionally, to depict a component selection strategy based on traditional features of the time-/frequency domain, we also applied the CASCSEL algorithm proposed earlier by our group [10]. It combines two approaches: on the one hand to exclude unsuitable components (by identifying artifact components), and on the other hand to select single suitable com-

ponents among the residual components. It can be briefly described according to the following three-step procedure: (1) estimate a spectral power ratio between low-frequency content P_{LF} (0.1 Hz to 5 Hz) and high-frequency content P_{HF} (5 Hz to 40 Hz) and exclude channels, which show less high-frequency content $P_{HF}/P_{LF} < 1$, (2) reintroduce/amplify fundamental oscillations related to the heart rate by filtering inspired by the Pan-Tompkins QRS detector and again test for the spectral power ratio but this time in reverse direction excluding components which show $P_{HF}/P_{LF} > d$ (with d an adaptive threshold, P_{LF} (0.5 Hz to 5 Hz) and P_{HF} (5 Hz to 30 Hz)) and (3) select the single component based on the power distribution in the low-frequency band (0.5 Hz to 5 Hz).

D. Evaluation of Selection Performance

The target of the component selection after the BSS was to select a single output component for further evaluation. In the selected BSS component, heartbeats were detected by applying our customized QRS-detector (see Section III-B), where the QRS-detector’s refractory period was set to 0.3 s. The performance of the selection was assessed by the heartbeat detection accuracy (ACC) of the selected BSS output component for each segment. The accuracy was obtained by comparing the manual QRS annotations from the reference ECG with the QRS detections estimated from the component as follows [10]:

$$ACC = \frac{TP}{TP + FP + FN} \quad (5)$$

In the case of the aECG, the pathologic beats were also expected to contribute to the true positive (TP) detections and were considered false positive (FP) or false negative (FN) otherwise (no true negative beats allowed).

In order to make a benchmark comparison to the input data without the BSS processing and selection routines, an average input ACC (Av.Input) is provided as the average ACC of all input leads of a segment using the same detector.

The statistical analysis of the accuracies was conducted separately for the textile, capacitive and arrhythmia ECG data. The acquired groups of accuracies (Av.Input, each BSS component selector) were pairwise compared by Wilcoxon’s signed-rank test after testing for significant differences between all groups by applying the Friedman test and assessing homoscedasticity of the groups by the Brown-Forsythe-test. To ensure independence within each group, the statistical analysis was calculated for subject-wise averaged accuracies ($N = 10$ resp. $N = 48$ for aECG data). As effect size measure for the p-values obtained from Wilcoxon’s signed-rank test, Cohen’s U1 including its 95%-confidence interval (CI) was calculated with bootstrapping ($N = 1000$) [35]. Since it assesses relative amounts of group elements being larger/smaller than opposing group maxima/minima, respectively, its interpretation is straightforward. A maximum effect ($U1 = 1$) is achieved if every group element of one group is larger than all elements of another group. No effect equals $U1 = 0$.

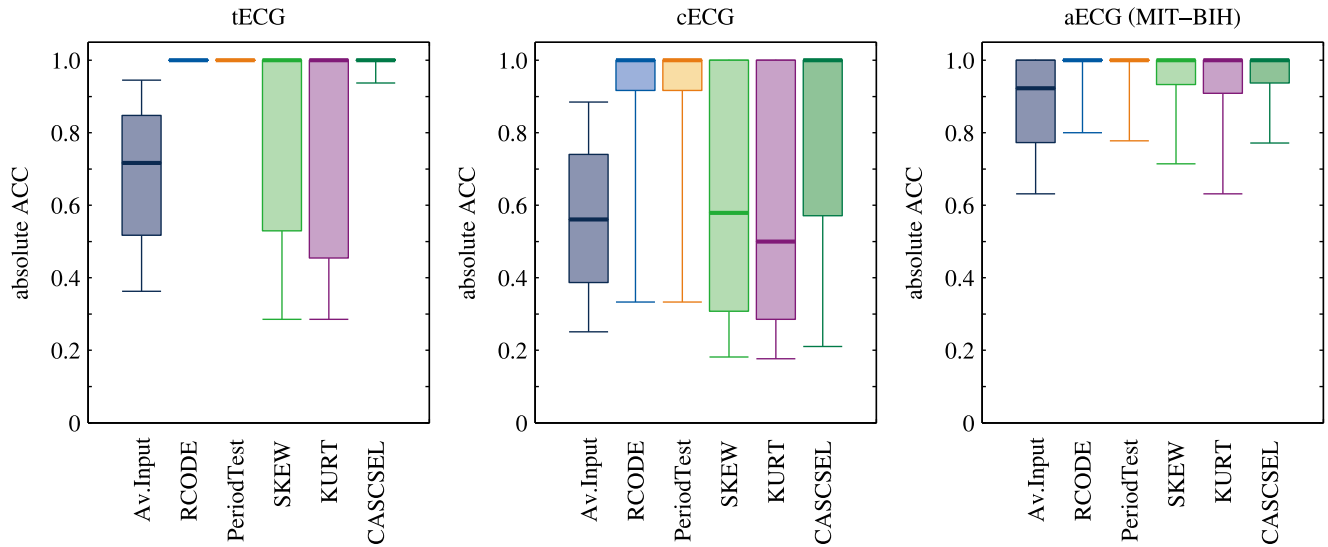


Fig. 5. Heartbeat detection accuracy ACC for each segment and subject ($N = 10$ resp. $N = 48$ for aECG data). Shown are the average input ACC (Av.Input) of the respective ECG input leads and the selections results of the RCODE, PeriodTest, Skewness (SKEW), Kurtosis (KURT) and Cascaded (CASCSEL) output component selectors. The whisker length is defined as 10% and 90% percentile, respectively. No outliers are shown. Subject-wise averaged results can be found in Tables I–III.

TABLE I
PAIRWISE RESULTS FOR tECG DATA

ACC	Group	Av.Input	RCODE	PeriodTest	SKEW	KURT	CASCSEL
0.687 ± 0.164	Av. Input		1 [1,1]	1 [1,1]	0.25 [0.15,0.6]	0.15 [0.1,0.5]	0.9 [0.75,1]
0.983 ± 0.014	RCODE	< 0.01		0.15 [0.1,0.4]	1 [1,1]	1 [1,1]	0.2 [0.1,0.4]
0.983 ± 0.011	PeriodTest	< 0.01	0.85		1 [1,1]	1 [1,1]	0.15 [0.1,0.4]
0.818 ± 0.110	SKEW	< 0.01	< 0.01	< 0.01		0.15 [0.1,0.35]	0.8 [0.65,1]
0.791 ± 0.129	KURT	0.06	< 0.01	< 0.01	< 0.01		0.8 [0.65,1]
0.972 ± 0.028	CASCSEL	< 0.01	0.04	0.06	< 0.01	< 0.01	

ACCs are shown as mean \pm standard deviation, p-values (below main diagonal) from Wilcoxon's signed-rank tests on subject-wise means ($N = 10$) and effect size (above main diagonal) Cohen's U1 and 95% CIs of U1 [35] in brackets.

IV. RESULTS

Fig. 5 shows boxplots of the accuracies obtained after selecting a single output component after spatio-temporal BSS application by using five different selectors (RCODE, PeriodTest, SKEW, KURT, CASCSEL) for three different datasets (tECG, cECG, aECG) without subject-wise averaging. The boxplots also show the average input accuracy (Av.Input) before BSS application to highlight the potential of BSS application in the context of the component selection. The Friedman test on subject-wise averaged ACCs on the tECG data shows highly significant differences between the groups ($p < 0.001$) as well as for cECG and aECG data. Brown-Forsythe-test proves homoscedasticity for the cECG and aECG data. Pairwise post-hoc tests including effect size measure Cohen's U1 and its 95% CI are shown in the Tables I–III.

The pairwise comparisons between the average input accuracy (Av.Input) and any component selection after spatio-temporal BSS show an unambiguous benefit of the BSS application with the subsequent component selection. Despite the Kurtosis selector for tECG and the Skewness and Kurtosis selector for cECG data, we find highly significant ACC increases by the selected BSS component compared to the average of input channels. Large effects (effect sizes) are obtained especially for

the peak-detection-based selectors (RCODE, PeriodTest) and the CASCSEL selector in tECG and cECG data. However, for tECG and cECG data, the application of higher order moments selection (SKEW, KURT) is not able to provide significantly higher ACC after BSS compared to the average of input channels.

Pairwise comparison of the peak-detection-based selectors (RCODE, PeriodTest) with the other selectors based on higher order moments or frequency-domain-features shows that the peak-detection-based methods significantly outperform the other approaches for all datasets. Large effects can especially be proven for tECG and cECG data. No significant difference of the RCODE/PeriodTest algorithm can be obtained in the case of the arrhythmia data in comparison to the Skewness selector. However, the average difference achieved in the output ACC (see Table III) between RCODE/PeriodTest and SKEW is 1.5% and 1.2%, respectively, in favor of the peak-detection-based methods. The Skewness selector always significantly outperforms the Kurtosis selector, too.

When comparing the peak-detection-based selectors (RCODE, PeriodTest) against each other, no significant difference between the obtained ACC of the respectively selected components can be found for tECG and cECG data. Despite being of very small absolute value, a significant difference in favor

TABLE II
PAIRWISE RESULTS FOR cECG DATA

ACC	Group	Av.Input	RCODE	PeriodTest	SKEW	KURT	CASCSEL
0.566 ± 0.136	Av. Input		0.85 [0.7,1]	0.9 [0.75,1]	0.25 [0.15,0.45]	0.1 [0.1,0.35]	0.7 [0.55,1]
0.867 ± 0.092	RCODE	< 0.01		0.1 [0.1,0.3]	0.7 [0.55,1]	0.8 [0.65,1]	0.3 [0.2,0.58]
0.868 ± 0.093	PeriodTest	< 0.01	0.77		0.7 [0.55,1]	0.8 [0.65,1]	0.3 [0.2,0.6]
0.629 ± 0.107	SKEW	0.08	< 0.01	< 0.01		0.3 [0.15,0.5]	0.6 [0.5,1]
0.584 ± 0.127	KURT	0.49	< 0.01	< 0.01	< 0.01		0.6 [0.5,1]
0.793 ± 0.064	CASCSEL	< 0.01	< 0.01	< 0.01	< 0.01	< 0.01	

ACCs are shown as mean ± standard deviation, p-values (below main diagonal) from Wilcoxon's signed-rank tests on subject-wise means (N = 10) and effect size (above main diagonal) Cohen's U1 and 95% CIs of U1 [35] in brackets.

TABLE III
PAIRWISE RESULTS FOR aECG (MIT-BIH) DATA

ACC	Group	Av.Input	RCODE	PeriodTest	SKEW	KURT	CASCSEL
0.871 ± 0.100	Av. Input		0.16 [0.10,0.33]	0.17 [0.12,0.30]	0.08 [0.05,0.23]	0.06 [0.03,0.19]	0.06 [0.03,0.23]
0.948 ± 0.065	RCODE	< 0.001		0.01 [0.01,0.04]	0.01 [0.01,0.08]	0.01 [0.01,0.17]	0.01 [0.01,0.09]
0.945 ± 0.067	PeriodTest	< 0.001	0.01		0.02 [0.01,0.07]	0.02 [0.01,0.14]	0.01 [0.01,0.09]
0.933 ± 0.083	SKEW	< 0.001	0.21	0.67		0.01 [0.01,0.10]	0.01 [0.01,0.08]
0.917 ± 0.095	KURT	< 0.001	< 0.01	0.02	< 0.001		0.01 [0.01,0.13]
0.942 ± 0.067	CASCSEL	< 0.001	0.01	0.16	0.91	0.06	

ACCs are shown as mean ± standard deviation, p-values (below main diagonal) from Wilcoxon's signed-rank tests on subject-wise means (N = 48) and effect size (above main diagonal) Cohen's U1 and 95% CIs of U1 [35] in brackets.

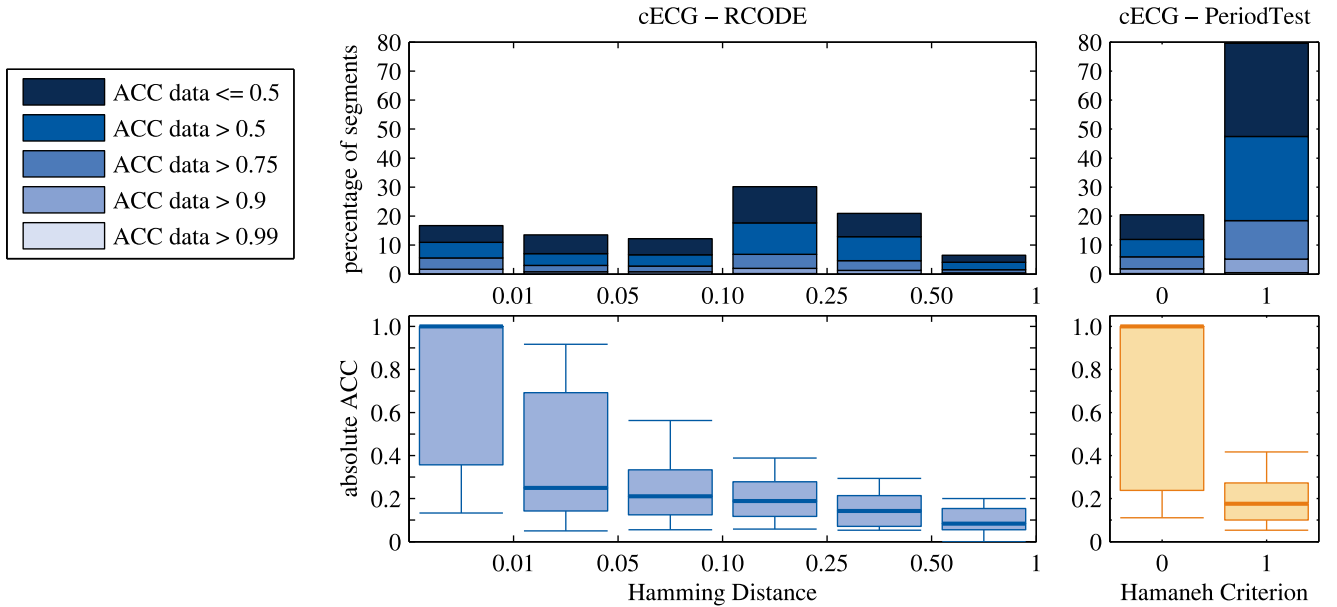


Fig. 6. Comparison between the modified Hamming distance gathered from the RCODE algorithm with the periodicity criterion according to the PeriodTest algorithm for the cECG data (whisker length marks 10% and 90% percentile, no outliers are shown). As comparative measure (y-axis) serve the ACC that is obtained from components' peak detections with respective Hamming distance/Hamaneh Criterion (x-axis). All available BSS output components are assessed (not only the selected components). A histogram shows the data distribution with respect to the input data quality (average ACC).

of RCODE is achieved for the aECG data. An insight into the direct comparison between RCODE and PeriodTest and their respective selection criteria, modified Hamming Distance and the Hamaneh periodicity criterion, is given in Figs. 6 and 7. The figures show the accuracy of any output component (i.e. its peak detections) given its selection measure for all available output components after BSS. The variance of the output ACC given $d_H/HC = 0$ underlines the necessity of applying an additional criterion (i.e. *AltSkew*) for selecting among the components

classified as suitable candidates by RCODE/PeriodTest. In the case of the cECG data (Fig. 6), the candidates for selection of the cardiac component (modified Hamming distance or Hamaneh criterion equals zero) show a higher first quartile in the according RCODE boxplot (ACC > 0.35) compared to the PeriodTest boxplot (ACC < 0.25). Fig. 7 shows the same assessment for the aECG data. In this case, the RCODE algorithm shows a slight advantage regarding the amount of data accessed as good cardiac component candidates. The histogram shows around 10%

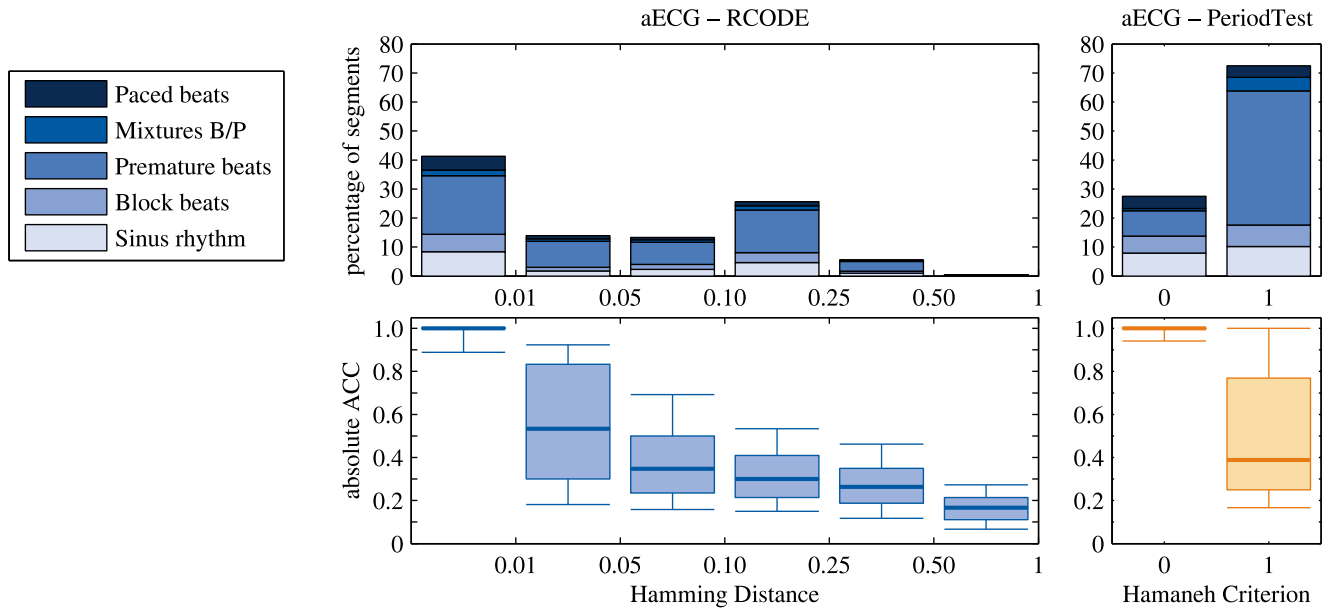


Fig. 7. Comparison between the modified Hamming distance gathered from the RCODE algorithm with the periodicity criterion according to the PeriodTest algorithm for the aECG data of the MIT-BIH database (whisker length marks 10% and 90% percentile, no outliers are shown). As comparative measure (y-axis) serve the ACC that is obtained from components' peak detections with respective Hamming distance/Hamaneh Criterion (x-axis). All available BSS output components are assessed (not only the selected components). A histogram shows the data distribution with respect to the rhythm/arrhythmia type.

more components achieving modified Hamming distance equal to zero compared to the components classified as periodic using the Hamaneh criterion with comparable ACC.

V. DISCUSSION

A. The Potential of Spatio-Temporal BSS

BSS in general is considered an appropriate tool for the processing of measurements imposing non-predictable and varying signal qualities across multiple channels (as exemplarily indicated in Figs. 1(a) and 2(a)). Moreover, spatio-temporal BSS is a powerful processing technique which combines spatial-filtering of multichannel data with channel-wise adaptive FIR filtering all guided by the concept of statistical independence [9]. Although it has been proven to successfully compete against the standard BSS [4], its application to cardiac signal processing is addressed only by limited number of researchers, so far [4], [9], [10], [36]. This may be attributed to the lack of robust selectors of components of interest (i.e. the cardiac component), namely for solving permutation indeterminacy, a problem intrinsic to the BSS. Especially, spatio-temporal BSS generates a vast amount of output components after its usage. Particularly, a very large number of temporal filter coefficients is proposed in [36]. At the same time, even pure spatial BSS (standard BSS) often requires complex selection routines of cascaded structure or pre-computed thresholds. Pre-trained templates are seldom transferable over datasets of different nature [11], [16], [17]. On the other hand, using non-symmetric BSS approaches like projection pursuit [9] which estimates output components one-by-one still involves the problem of deciding whether the component of interest has already been extracted.

We have shown, that component selection methods based on peak detections (RCODE, PeriodTest) and their rhythm evaluation regarding potential cardiac behaviour are capable of handling spatio-temporal BSS outputs of different data nature (i.e. tECG, cECG, aECG). This can be seen from Fig. 5, where for tECG and aECG data both median and inter-quartile-range (IQR) show output accuracies of selected components being $ACC = 1$. Also, the highly distorted cECG data achieve an IQR $ACC > 0.9$. This finding is underlined by the pairwise comparisons of these selectors with the average input quality (Tables I–III), always significantly increasing ACC. Efficient usage of spatio-temporal BSS, thus, becomes possible.

B. Selection Strategies

One major problem of automatically selecting a single (desired) component after BSS application is given by undesired components (e.g., artifact components) resembling features initially chosen to characterize the desired component. In particular, this is relevant for higher order moments, which are heavily affected by outliers or time-/frequency based features [25]. Moreover, both types of features may vary in absolute and relative values between datasets of different origin [37], which renders an according feature selection to be even more complicated. We observed the susceptibility of higher order moments to artifacts especially in the minimal-conductive ECG datasets (tECG and cECG, see Fig. 5), where artifacts are likely to occur (e.g., see Fig. 1(a)). In pairwise comparisons (Tables I and II) even a decrease in ACC after BSS application and the subsequent selection was obtained by using Skewness or Kurtosis selectors (with outlier removal). For an almost artifact-free ECG setting (aECG) the higher order moments (i.e. Skewness) performed

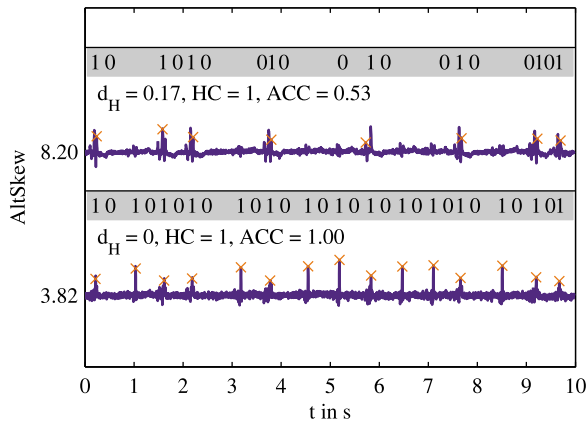


Fig. 8. Two different BSS output component examples of one aECG recording. The lower panel shows the RCODE selection and the respective PeriodTest selection is depicted in the upper panel. The corresponding modified Hamming distance (d_H), Hamaneh criterion (HC) and beat detection accuracy (ACC) is provided. The sparse code sequence is indicated above each component and the QRS detections obtained from the customized peak detector are marked as orange crosses. The y-axis shows the *AltSkew* measure.

well and no significant difference compared to other selectors was observed. This highlights the limitations of higher order moments as the BSS component selector in distorted ECG settings. Still, Skewness showed better performance than Kurtosis, which is in accordance with [4].

Nevertheless, a selector based on peak detections can also be misguided, since its performance is given by: (1) the detection performance prior to selection, and (2) the detection performance after selection. Both performances are not necessarily the same, since, e.g. prior to selection, our detector was designed to be more sensitive to artifacts compared to the post-selection detector. Also, periodic artifacts (such as those included in the measurement protocol of the assessed cECG data) can cause an artifact component being a good cardiac candidate according to the selection criterion. The large IQR (Fig. 6) of components showing Hamming distance or Hamaneh criterion equals zero for the cECG data is a possible consequence. However, Fig. 6 shows the detection accuracy in all available output components, whereas Fig. 5 depicts the results only for the selected ones. The largely decreased IQR in Fig. 5 (cECG) compared to Fig. 6 supports the usability of our additional selection criterion *AltSkew* in the case of multiple cardiac component candidates after peak detection evaluation and underlines its necessity. In the case of arrhythmia, which can also hamper periodicity tests based on peak detections, the advantage of our advanced code manipulation and assessment (RCODE) compared to the simple periodicity test (PeriodTest) emerges. Fig. 8 underlines this finding by means of two BSS components after processing aECG. The upper component was selected by PeriodTest solely based on *AltSkew*, because no output component could be classified as periodic according to the Hamaneh criterion HC ($HC = 1 \forall$ components). Accordingly, using *AltSkew* alone fails to select the proper component in this case. The lower component (Fig. 8)

was selected by RCODE according to its modified Hamming distance $d_H = 0$ and shows maximum $ACC = 1$. Thus RCODE shows a higher capability to select cardiac components in the case of arrhythmia. Also, RCODE explicitly tries to compensate for arrhythmia originating from blocks before rhythm evaluation (but it doesn't compensate for fibrillation type arrhythmia). Whereas this is not relevant for the healthy subjects in the tECG and cECG data, for the aECG data we obtain a slightly but significantly higher output ACC using RCODE (Table III). Moreover, around 10% more components (Fig. 7) can be exploited of the aECG data showing Hamming distance equal to zero compared to the PeriodTest-selected components. Nevertheless, it should be noted that the BSS analysis of the two-lead ECGs in the aECG data comprises a less complicated component selection problem in BSS's permutation indeterminacy, as compared to the analysis of the tECG and cECG data. However, it is assumed, that the equivalent BSS processing for all data using the same amount of time lags in BSS input construction brings along comparable BSS component characteristics as precondition for the selection problem. Accordingly, the aECG results are considered exemplary for arrhythmia data originating from minimum-contact techniques.

VI. CONCLUSION

We have investigated the performance of several strategies for automatically selecting a single component (namely the cardiac component) after applying spatio-temporal BSS to ECG recordings of different nature. We tested component selectors based on the evaluation of peak detections from a rhythmical point of view and compared this to the classical usage of higher order moments and frequency domain features for this purpose.

We observed, that the usage of peak detections for solving permutation indeterminacy after BSS in the ECG context is to be preferred over the usage of higher order moments or frequency-domain features. The application of a sophisticated evaluation of peak detections (RCODE) shows an advantage over simple periodicity tests (PeriodTest) in special applications like arrhythmia ECG. In the case of using higher order moments for the selection of spatio-temporal BSS components, the Skewness is to be preferred over the Kurtosis.

Spatio-temporal BSS processing is highly capable of processing ECGs with large distortions like minimal-conductive ECGs as textile or capacitive ECG. The disadvantage of spatio-temporal BSS is a large number of output components obtained after processing, which causes component selection after BSS to be difficult. However, the availability of methods (RCODE, PeriodTest) being able to handle large amounts of BSS output components and, nevertheless, selecting the best cardiac component with high certainty, facilitates utilizing the potential of spatio-temporal BSS for processing highly distorted ECGs. This promotes the usage of spatio-temporal BSS for accessing cardiac information from minimum-contact ECGs as textile or capacitive ECG. Future work should address the evaluation of the obtained results for arrhythmia ECG data measured with minimum-contact ECG techniques.

REFERENCES

- [1] K. Hoffmann and R. Ruff, "Flexible dry surface-electrodes for ECG long-term monitoring," in *Proc. 29th Annu. Int. Conf. IEEE Eng. Med. Biol. Soc.*, Lyon, France, 2007, pp. 5739–5742.
- [2] M. Walter *et al.*, "The smart car seat: Personalized monitoring of vital signs in automotive applications," *Pers. Ubiquitous Comput.*, vol. 15, no. 7, pp. 707–715, 2011.
- [3] Y. Chi *et al.*, "Dry-contact and noncontact biopotential electrodes: methodological review," *IEEE Rev. Biomed. Eng.*, vol. 3, pp. 106–119, 2010, doi: [10.1109/RBME.2010.2084078](https://doi.org/10.1109/RBME.2010.2084078).
- [4] U. Wiklund *et al.*, "Adaptive spatio-temporal filtering of disturbed ECGs: A multi-channel approach to heartbeat detection in smart clothing," *Med. Biol. Eng. Comput.*, vol. 45, no. 6, pp. 515–523, 2007.
- [5] C. Antink *et al.*, "Beat-to-beat heart rate estimation fusing multimodal video and sensor data," *Biomed. Opt. Express*, vol. 6, no. 8, pp. 2895–2907, 2015.
- [6] A. Hyvärinen, "Fast and robust fixed-point algorithms for independent component analysis," *IEEE Trans. Neural Netw.*, vol. 10, no. 3, pp. 626–634, May 1999.
- [7] N. Östlund *et al.*, "Adaptive spatio-temporal filtering of multichannel surface EMG signals," *Med. Biol. Eng. Comput.*, vol. 44, no. 3, pp. 209–215, 2006.
- [8] C. James and C. Hesse, "Independent component analysis for biomedical signals," *Physiol. Meas.*, vol. 26, no. 1, pp. R15–R39, 2005.
- [9] N. Östlund *et al.*, "Adaptive spatio-temporal filtration of bioelectrical signals," in *Proc. 27th Annu. Int. Conf. IEEE Eng. Med. Biol. Soc.*, Shanghai, China, 2005, vol. 27, pp. 5983–5986.
- [10] D. Wedekind *et al.*, "Cascaded output selection for processing of capacitive electrocardiograms by means of independent component analysis," in *Proc. 8th Int. Workshop Sensor Data Fusion*, Bonn, Germany, 2013, pp. 1–6.
- [11] T. He *et al.*, "Application of independent component analysis in removing artefacts from the electrocardiogram," *Neural Comput. Appl.*, vol. 15, no. 2, pp. 105–116, 2006.
- [12] M. Milanese *et al.*, "Independent component analysis applied to the removal of motion artifacts from electrocardiographic signals," *Med. Biol. Eng. Comput.*, vol. 46, no. 3, pp. 251–261, 2008.
- [13] J. Kuzilek *et al.*, "Independent component analysis and decision trees for ECG holter recording de-noising," *PLoS One*, vol. 9, no. 6, pp. e98450–1–e98450–9, 2014.
- [14] A. Rashid *et al.*, "Electrocardiogram signal processing for baseline noise removal using blind source separation techniques: A comparative analysis," in *Proc. 4th Int. Conf. Mach. Learn. Cybern.*, Guilin, China, 2011, pp. 1756–1761.
- [15] J. Kuzilek and L. Lhotska, "Electrocardiogram beat detection enhancement using independent component analysis," *Med. Eng. Phys.*, vol. 35, no. 6, pp. 704–711, 2012.
- [16] J. Rieta *et al.*, "Atrial activity extraction for atrial fibrillation analysis using blind source separation," *IEEE Trans. Biomed. Eng.*, vol. 51, no. 7, pp. 1176–1186, Jul. 2004.
- [17] A. Acharyya *et al.*, "Robust channel identification scheme: solving permutation indeterminacy of ICA for artifacts removal from ECG," in *Proc. 32nd Annu. Int. Conf. IEEE Eng. Med. Biol. Soc.*, Buenos Aires, Argentina, 2010, pp. 1142–1145.
- [18] J. Krug *et al.*, "ECG-based gating in ultra high field cardiovascular magnetic resonance using an independent component analysis approach," *J. Cardiovascular Magn. Reson.*, vol. 15, no. 104, pp. 1–13, 2013.
- [19] G. Tsouri and M. Ostertag, "Patient-specific 12-lead ECG reconstruction from sparse electrodes using independent component analysis," *IEEE J. Biomed. Health Informat.*, vol. 18, no. 2, pp. 476–482, Mar. 2014.
- [20] C. Di Maria *et al.*, "An algorithm for the analysis of fetal ECGs from 4-channel non-invasive abdominal recordings," in *Proc. 40th Comput. Cardiol. Conf.*, Zaragoza, Spain, 2013, pp. 305–309.
- [21] D. Wedekind *et al.*, "Processing of capacitive electrocardiograms by back transformation of selected independent components," in *Proc. Workshop Innovative Verarbeitung Bioelektrischer und Biomagnetischer Signale*, Berlin, Germany, 2014, pp. 31–32.
- [22] F. Andreotti *et al.*, "Robust fetal ECG extraction and detection from abdominal leads," *Physiol. Meas.*, vol. 35, no. 8, pp. 1551–1567, 2014.
- [23] M. Varanini *et al.*, "A multi-step approach for non-invasive fetal ECG analysis," in *Proc. 40th Comput. Cardiol. Conf.*, Zaragoza, Spain, 2013, pp. 281–284.
- [24] M. Hamaneh *et al.*, "Automated removal of EKG artifact from EEG data using independent component analysis and continuous wavelet transformation," *IEEE Trans. Biomed. Eng.*, vol. 61, no. 6, pp. 1634–1641, Jun. 2014.
- [25] D. Wedekind *et al.*, "Sparse coding of cardiac signals for automated component selection after blind source separation," in *Proc. 43rd Comput. Cardiol. Conf.*, Vancouver, BC, Canada, 2016, pp. 1–4.
- [26] C. James and O. Gibson, "Temporally constrained ICA: An application to artifact rejection in electromagnetic brain signal analysis," *IEEE Trans. Biomed. Eng.*, vol. 50, no. 9, pp. 1108–1116, Sep. 2003.
- [27] J. Lee *et al.*, "Temporally constrained ICA based foetal ECG separation," *Electron. Lett.*, vol. 41, no. 21, pp. 1158–1160, 2005.
- [28] A. Goldberger *et al.*, "PhysioBank, PhysioToolkit, and PhysioNet: Components of a new research resource for complex physiologic signals," *Circulation*, vol. 101, no. 23, pp. e215–e220, 2000.
- [29] G. Moody and R. Mark, "The impact of the MIT-BIH arrhythmia database," *IEEE Eng. Med. Biol. Mag.*, vol. 20, no. 3, pp. 45–50, May/Jun. 2001.
- [30] F. Chiarugi *et al.*, "Adaptive Threshold QRS Detector with Best Channel Selection Based on a Noise Rating System," in *Proc. 34th Comput. Cardiol. Conf.*, Durham, NC, USA, 2007, pp. 157–160.
- [31] R. Sameni, "The open-source electrophysiological toolbox (OSET), version 2.1," 2010. [Online]. Available: www.oset.ir
- [32] P. Pan and W. Tompkins, "A real-time QRS detection algorithm," *IEEE Trans. Biomed. Eng.*, vol. BME-32, no. 3, pp. 230–236, Mar. 1985.
- [33] E. Christinaki *et al.*, "Comparison of blind source separation algorithms for optical heart rate monitoring," in *Proc. 4th Mobihealth*, Athens, Greece, 2014, pp. 339–342.
- [34] S. Walsh, "Some nonparametric tests of whether the largest observations of a set are too large or too small," *Ann. Math. Statist.*, vol. 21, no. 4, pp. 583–592, 1950.
- [35] H. Hentschke and M. Stüttgen, "Computation of measures of effect size for neuroscience data sets," *Eur. J. Neurosci.*, vol. 34, no. 12, pp. 1887–1894, 2011.
- [36] Y. Sun *et al.*, "Motion-compensated noncontact imaging photoplethysmography to monitor cardiorespiratory status during exercise," *J. Biomed. Opt.*, vol. 16, no. 7, 2011, Art. no. 077 010.
- [37] U. Acharya *et al.*, "Heart rate variability: A review," *Med. Biol. Eng. Comput.*, vol. 44, no. 12, pp. 1031–1051, 2006.